Giftet Inc.
Journal of Geolocation, Geo-information, and Geo-intelligence
Volume 2023, article ID 2023071602, 13 pages
http://doi.org/10.18610/JG3.2023.071602

*Technical Report*

# Discrete vs. Continuous Carrier Tracking Loop with Large BnT: Part 2, Implementation and Testing[i]

**Ilir F. Progri[1], Clifford W. Kelley[2], Guojiang Gao[3], William R. Michalson[4], Jinling Wang[5], and John Lavrakas[6]**

[1]*Giftet Inc., 5 Euclid Ave. #3, Worcester, MA 01610, USA*

[2]*Open Source GPS, CA, USA*

[3]*University of Calgary, Canada*

[4]*Electrical and Computer Engineering Department, Worcester Polytechnic Institute, Worcester, MA 01609, USA*

[5]*University of New South Wales, Sydney, Australia*

[6]*Advanced Research Corp., Newport, OR*

*ORCID: 0000-0001-5197-1278*

Correspondence should be addressed to Ilir Progri; iprogri@giftet.com.

Received June 7, 2023; Revised June 8, 2023-July 10, 2023, Accepted July 16, 2023; Published November 1, 2023.

Editor-in-Chief/ Senior Scientific Editor: Ilir F. Progri



*Abstract*—In part one of the journal paper, we performed the analysis of the discrete vs. continuous carrier tracking loop with large $B_nT$ (in Progri et al 2023). In this technical report we verified the theory (in Progri et al. 2023) with data from tests with the Open-Source GPS software receiver emulation (theoretical or ideal signal) and then with the GP2015/2021 hardware (with a real GPS signal coming from a GPS satellite). The results presented include the experimental data that were employed to validate our theoretical approach (in Progri et al 2023). According to our analysis (in Progri et al 2023) for $0 < B_nT < 0.3329$ the carrier tracking is stable; however, for $0.3329 < B_nT \leq 0.5$ the carrier tracking is marginally stable; i.e., it stable in short term or for a few seconds and unstable in the long term or for many seconds, minutes, hours etc. From the experimental data, recorded by Mr. Kelly, we were able to confirm that for $B_nT \leq 0.3$ the carrier tracking loop was stable, for $B_nT = 0.5$ the carrier tracking loop was marginally stable and $B_nT = 1$ the carrier tracking loop was unstable. Therefore, there appears to be a flawless agreement between theory (in Progri et al 2023) and the experimental results from implementation and testing.

*Index Terms*—Carrier tracking, integration time, loop bandwidth, implementation, testing, Open-Source GPS.

## 1 Introduction

In part one of the journal paper, it became clear that the product of the noise bandwidth with the integration time has a significant effect on the stability of the tracking loops be it delay lock loop (DLL) for code tracking or phase or frequency locked loop (PLL or FLL) for carrier tracking in Progri et al. (2023, [2]).

The test setup for this journal paper was not accidental. In Progri et al. (1998, [3]) a similar test setup was proposed that considered an ideal scenario with no mutual coupling and channel error and then with frequency independent mutual coupling and channel errors and then finally with frequency dependent mutual coupling and channel errors.

In Upadhyay et al. (1999, [4]) it was then Ph.D. student Progri who designed, developed, simulated, and implemented successfully the NASA Phase II Small Business Innovative Research (SBIR) Docking Attitude and Navigation System (DANS) which earned him a prestigious Mayflower Award in October of 1998.

In Progri et al. (2001, [4]) which was later published in the journal paper Progri et al. (2002, [5]) and then published in Chap. 6 in Progri (2011, [12]) an implementation test setup that used the sum, product, and various signal processing adaptive functions was employed successfully.

In Progri et al. (2002, [6]) a complete analysis, design, simulation of a C-CDMA indoor geolocation system was proposed and successfully simulated for the first time in MATLAB, which became the center piece of Dr Progri, Ph.D. dissertation in Progri (2003, [9]).

In Progri et al. (2003, [8]) which was later published in the journal paper Progri et al (2004, [10]) a complete OFDMA indoor geolocation system was proposed, analyzed, and simulated successfully in MATLAB. The simulation test setup was very similar to the one proposed in this technical report.

From 1998 until 2007 Dr. Progri performed many successful research projects which are not reference in this technical report but the experience drawn from these projects had a lasting impact in formation of his sound engineering doctrine, practice, and foundation.

The implementation and the test setup of this important project required careful and proven engineering practices to achieve the desired outcome.

Dr. Progri had successfully demonstrated that he was able to carry the analysis, modeling, simulation, and implementation step by step based on sound engineering practices, foundation.

The investigation proposed in this technical report was a very natural extension from the experience dawn from Dr. Progri extensive research and publication from 1998 until 2007. In this technical report, Dr. Progri proposed the test setup which Mr. Kelly implemented in this technical report.

In order to investigate this inconsistency and be able to explain the lack of consistency between the published theory and experimental data we implemented the carrier-tracking loop for Open-Source GPS using the same integration time for the carrier and code loops equal to the 20 ms data period. First, we tracked in accumulated carrier phase by setting the loop bandwidth approximately equal to 25 Hz, which produces a $B_nT$ of 0.5. Initially the carrier tracking loop appeared to work well but, later on the position and to a larger extent the velocity fixes accumulated more and more error. Second, since it was known that this loop works well with an integration time of 1ms it motivated (or gave us the incentive) us on to look into this phenomenon in greater detail.

Based on the analysis performed in Progri et al. (2023, [2]) we verified the influence of the $B_nT$ on the code and carrier tracking loop stability with data from tests with the Open-Source GPS software receiver emulation (theoretical or ideal signal) and then with the GP2015/2021 hardware (with a real GPS signal coming from a GPS satellite). The results presented include our theoretical approach and the experimental data. According to our analysis it appears that for $0 < B_nT < 0.3329$ the carrier tracking is stable; however, for $0.3329 < B_nT \leq 0.5$ the carrier tracking is marginally stable; i.e., it stable in short term or for a few seconds and unstable in the long term or for many seconds, minutes, hours etc. From the experimental data we were able to confirm that for $B_nT \leq 0.3$ the carrier tracking loop was stable, for $B_nT = 0.5$ the carrier tracking loop was marginally stable, and for $B_nT = 1$ the carrier tracking loop was unstable.

The paper is organized in the following manner. First, we present results that include the theoretical signal without noise and clock errors and the real GPS with noise and clock errors. Second, we present a summary and conclusion section. Third, we provide a future work section. Appendix A contains the implementation results with no noise and no clock error, Appendix B presents the implementation results of the real GPS signal.

TABLE I: BANDWIDTH INTEGRATION TIME PRODUCT; NO NOISE INFINITE BANDWIDTH/FOR A REAL GPS SIGNAL (S = STABLE, M = MARGINALLY STABLE, U = UNSTABLE)

| | $B_n$ (Hz) | | | | | | |
|---|---|---|---|---|---|---|---|
| $T$ (ms) | 1 | 2 | 5 | 10 | 15 | 25 | 50 |
| 1 | 0.001 (S) | 0.002 (S) | 0.005 (S) | 0.01 (S) | 0.015 (S) | 0.025 (S) | 0.05 (S) |
| 2 | 0.002 (S) | 0.004 (S) | 0.01 (S) | 0.02 (S) | 0.03 (S) | 0.05 (S) | 0.1 (S) |
| 4 | 0.004 (S) | 0.008 (S) | 0.02 (S) | 0.04 (S) | 0.06 (S) | 0.1 (S) | 0.2 (S) |
| 5 | 0.005 (S) | 0.01 (S) | 0.025 (S) | 0.05 (S) | 0.075 (S) | 0.125 (S) | 0.25 (S) |
| 10 | 0.01 (S) | 0.02 (S) | 0.05 (S) | 0.1 (S) | 0.15 (S) | 0.25 (S) | 0.5 (S) |
| 20 | 0.02 (S) | 0.04 (S) | 0.1 (S) | 0.2 (S) | 0.3 (S) | 0.5 (M) | 1 (U) |

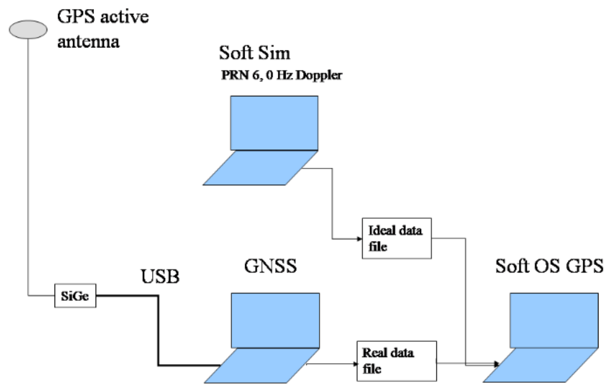


FIGURE 1: GP2021 experimental setup.

## 2 Experimental Setup and Results

Figure 1 depicts the GP2021 experimental setup, proposed by Dr. Progri and then implemented by Mr. Kelly, to test the value of the $B_nT$ product ranging from 0.001 to 1.

As explained in the introduction, this test setup was not accidental. It was envisioned by many years of experience, research, and development from Progri et al. (1998, [3]) until Progri et al. (2004, [10]) just to name a few similar, successful, and important projects. The test setup of this technical report was based on sound, firm engineering practices or foundation.

Table I contains the values of the $B_nT$ that were used for the two sets of the experimental setup. Further details of the experimental setup are given below. Results are produced utilizing two sets of scenarios (or experiments):

1. Theoretical (ideal) signal: no noise and no clock errors. The simplest test was the theoretical signal, which does neither contain any noise nor clock errors. The only real limitation on the tracking loop was the quantization of the carrier digitally controlled oscillator (DCO) frequency setting which is: 40MHz/7/2^27 or about 42.6 milli-Hz.
2. Real signal: with noise and clock errors. For this experimental setup Cliff recorded 60 sec of IF data from the SiGe with a 2-bit A/D, an IF at 4.1304 MHz sampled at 16.3676 MHz. The antenna was at a fixed location in Palos Verdes with a nearly clear view of the sky. It is just above the roof of Cliff's house so there is the possibility of multipath toward the west. The data was recorded on Dec 5, 2006 at 6:45 PM (see Progri et al. (2007,[1] )).

### *2.1 Theoretical signal: no noise and no clock errors*

The simplest test was the theoretical signal, which does neither contain any noise and nor any clock errors. The only real limitation on the tracking loop was the quantization of the carrier DCO frequency setting which is: 40MHz/7/2^27 or about 42.6 milli-Hz (see the results in Appendix A).

Table I contains a summary of the test results. As shown in Tab. I the product of $B_nT$ is less than one for 41 cases and one for one case. As indicated in Tab. I the system is stable when $B_nT < 1$ and unstable for $B_nT = 1$.

One set of experiments consists of forty-two combinations of the $B_nT$ product. For thirty-nine of these combinations that satisfy $B_nT \leq 0.3$ the theory and the experimental data with ideal signal agree flawlessly by indicating that the carrier tracking is stable. In order to examine and demonstrate the stability we have shown the signals at the input and output of the second order carrier and code tracking loop filter in Figs. 2 through 6.

Furthermore Figs. 2 through 4 show the in-phase and quadrature early and late carrier tracking for $T = 1$ ms and $B_n = 1$ Hz and different zoom aspects of the time scale. We can clearly note the symbol transition every 40 ms and all the symbols are rectangular (or square waves) and there in no anomaly in every symbol. The $C_2 = 0.0001 < 1$ which explains the stability of the second order carrier loop filter. We also notice that the early symbol is on the outside and the late symbol on the inside. Figures 5 through 7 show the output of the carrier and code tracking loops namely the carrier DCO and code DCO. Both the code and carrier DCO are stable and we also notice that the code DCO changes every multiple of 20 ms. The carrier DCO change however does not follow the 20 ms rule.

For the forty-second combination of the $B_nT$ product for which $B_nT = 1$ the theory and the experimental data with ideal signal agree flawlessly by indicating that the carrier tracking is unstable. In order to examine and demonstrate the stability we have shown the signals at the input and output of the second order carrier and code tracking loop filter in Figs. 8 through 13. Furthermore Figs. 8 through 10 show the in-phase and quadrature early and late carrier tracking for $T = 20$ ms and $B_n = 25$ Hz and different zoom aspects of the time scale. We can no longer recognize the symbol transition every 40 ms and all the symbols are no longer rectangular (or square waves) and there in a clear anomaly in every symbol. We also notice that the early symbol is on the outside and the late symbol on the inside. At 1.7 s the carrier loop goes from stable to unstable as a result of the divergence caused by the value of the $C_2 = 4.1814 \gg 1$ coefficient as predicted in the theory. Figures 5 through 7 show the output of the carrier and code tracking loops namely the carrier DCO and code DCO. Both the code and carrier DCO are stable and we also notice that the code DCO changes every multiple of 20 ms. The carrier DCO symbol transition change however does not follow the 20 ms rule.

## *2.2 Real GPS signal: with noise and clock errors*

For this experimental setup Cliff recorded 60 sec of IF data from the SiGe with a 2-bit A/D, an IF at 4.1304 MHz sampled at 16.3676 MHz. The antenna was at a fixed location in Palos Verdes with a nearly clear view of the sky. It is just above the roof of Cliff's house so there is the possibility of multipath toward the west. The data was recorded on Dec 5, 2006 at 6:45 PM (see Progri et al. (2007, [1])). (see the results in Appendix B)

Table I contains a summary of all the test results of the 42 combinations of the $B_nT$ product. As indicated in the summary Tab. I for 39 combinations of $B_nT$ product which $B_nT \leq 0.3$ the theory and the experimental data with real signal agree flawlessly by indicating that the carrier tracking is stable; however, for sixteen cases as indicated in Tab. I we observed larger variance of the phase noise. We will investigate the phase error later for these sixteen cases and try to come up with a detailed explanation. In order to examine and demonstrate the stability we have shown the signals at the input and output of the second order carrier and code tracking loop filter in Figs 14 through 19. Furthermore Figs 14 through 16 show the In-phase and Quadra-phase early and late carrier tracking for $T = 1$ ms and $B_n = 1$ Hz and different zoom aspects of the time scale. We can clearly note the symbol transition every 20 ms and all the symbols are rectangular (or square waves) and there is large noise in every symbol. The $C_2 = 0.0001 < 1$ which explains the stability of the second order carrier loop filter. We also notice that due to large observed phase noise the early symbol is no longer on the outside and the late symbol no longer on the inside but they overlap. Figures 17 through 19 show the output of the carrier and code tracking loops namely the carrier DCO and code DCO. Both the code and carrier DCO are stable and we also notice that the code DCO changes every multiple of 20 ms. The carrier DCO change however does not follow the 20 ms rule.

For the fortieth and forty-first combinations of the $B_nT$ product for which $B_nT = 0.5$ the theory and the experimental data with real signal agree flawlessly by indicating that the carrier tracking is marginally stable. In order to examine and demonstrate the stability we have shown the signals at the output of the second order carrier tracking loop filter in Fig. 20. As indicated in Fig. 20 the output of the carrier DCO is somewhat stable during the initial 4.88 seconds and then begins to slowly drift away. This phenomenon occurs because the value of the coefficient $C_2$ is ~ 1.7. The filter initially tries to maintain stability in the short term and later as the error begins to grow the filter output slowly diverges away.

For the forty-second combination of the $B_nT$ product for which $B_nT = 1$ the theory and the experimental data with real signal agree flawlessly by indicating that the carrier tracking is unstable. In order to examine and demonstrate the stability we have shown the signals at the input and output of the second order carrier and code tracking loop filter in Figs 20 through 26. Furthermore Figs 21 through Figs 23 show the In-phase and Quadra-phase early and late carrier tracking for $T = 20$ ms and $B_n = 25$ Hz and different zoom aspects of the time scale. We can no longer recognize the symbol transition every 20 ms and all the symbols are no longer rectangular (or square waves) and there is a clear anomaly in every symbol. We also notice that the early symbol is on the outside and the late symbol on the inside. At 1.95 s the carrier loop goes from stable to unstable as a result of the divergence caused by the value of the $C_2 = 4.1814 \gg 1$ coefficient as predicted in the theory. Figures 24 through 26 show the output of the carrier and code tracking loops namely the carrier DCO and code DCO. Although the code DCO is stable and we also notice that the code DCO changes every multiple of 20 ms, the carrier DCO is unstable in both short and long term as seen in Figs 25 and 26.

## 3 Conclusions

We have presented the discrete vs. continuous tracking loop with large $B_nT$ implementation and testing to a great deal of detail. In order to test out our theory we conducted two sets of experiments. Both sets of experiments consisted of forty-two experiments for which the values of $B_nT$ were taken from the $B_n \times T$ matrix shown in Tab. I. As shown in Tab. I for thirty-nine of these combinations $B_nT \leq 0.3$, for two combinations $B_nT = 0.5$ and for only one combination $B_nT = 1$ .:

1. For the first set of experiments an ideal signal was used; i.e., a signal without noise and clock errors.
2. For the second set of experiments a real GPS signal was used; i.e., a signal with noise and clock errors as received from a GPS antenna.
3. In both sets of experiments for all the combinations for which $B_nT \leq 0.3$ the output of the carrier loop was stable;
4. however, for two the combinations for which $B_nT = 0.5$ the output of the carrier loop was marginally stable for the only combination for which $B_nT = 1$ the output of the carrier DCO was unstable.

All these conclusions are in a complete agreement with what was initially predicted in our analysis in Progri et al. (2023, [2]).

Because the code loop carrier tracking bandwidth is so much smaller, we will almost never see the code loop become unstable for the values of $B_nT$ for which the carrier loop is unstable.

When $B_nT$ is close to one, signal tracking loops in a digital receiver will become unstable (as proved by Progri et al. (2023, [2])). Furthermore, even when $B_nT$ is much smaller than one, if the integration time T is very long, it is still possible that a digital receiver will crash in run, because the accumulated phase tracking errors induced by receiver dynamics and oscillator instability in one integration time interval may reach the tracking threshold (as proved by Gao (2007, [11])). In conclusion, for a digital GPS receiver, the expression for PLL/FLL tracking errors has to be modified.

The success of this project was not accidental. Dr. Progri had successfully demonstrated that he was able to carry the analysis, modeling, simulation, and implementation step by step based on sound engineering practices. Even in this very important topic in which there was a lack of agreement between the theory and practice, Dr. Progri led a successful team effort followed by sound and firm theoretical and practical engineering practices and foundation and provided the necessary guidance from the initial conception and the completion of this important project.

## 4 Acknowledgement

The publication of this work in the Giftet Journal of Geolocation, Geoinformation, and Geo-intelligence was supported by Giftet Inc. executive office as part of the pioneer publication Progri (2024, [13]).

The authors would like to thank The Open-Source GPS, The University of Calgary, Point Inc, WPI, The University of New South Wales, The Advanced Research Corp., and The Institute of Navigation for their continued support. The author would also like to thank the session chair and the program committee for accepting our paper.

## 5 References

[1] I. Progri, C.W. Kelley, G. Gao, W.R. Michalson, J. Wang, J. Lavrakas, "Discrete vs. continuous carrier tracking loop theory, implementation, and testing with large BnT," in *Proc. 20th Intr. Tech. Mtg. Sat. Div. ION (ION GNSS 2007)*, Fort Worth, TX, pp. 2584-2610, Sep. 2007, http://giftet.com/Progri/Progri_2007_09_02_ION_GNSS.pdf.

[2] I. Progri, C.W. Kelley, G. Gao, W.R. Michalson, J. Wang, J. Lavrakas, "Discrete vs. continuous carrier tracking loop with large BnT: part 1, theory," *J. Geol. Geoinfo. Geointel.,* vol. 2023, article ID 2023071601, 18 pg., Nov. 2023. DOI: http://doi.org/10.18610/JG3.2023.071601, http://giftet.com/JG3/2023/071601.pdf.

[3] I. Progri, B.W. Nicholson, D.M. Upton, T. Upadhyay, W.E. Vander Velde, "Impacts of frequency dependent mutual coupling and channel errors on digital beam-forming antenna performance," in *Proc. 11th Inter. Tech. Mtg. Sat. Div. ION (ION-GPS 1998)*, Nashville, TN, pp.

275-283, Sep. 1998, http://giftet.com/Progri/Progri_1998_09_027.pdf.

[4] T.N. Upadhyay, I. Progri, J. Lomas, J, Buckler, "Precision relative navigation for automated rendezvous and docking," in *Proc. Annual AAS Guidance & Control*, Breckenridge, CO, pp. 368-379, Feb. 1999, URL: http://giftet.com/Progri/Progri_1999_02_COA_AAS_Breckenridge_CO.pdf.

[5] I. Progri, G. Bogdanov, V.C. Ramanna, "An investigation of the adaptive temporal selective attenuator," in *Proc. 14th Inter. Tech. Mtg. Sat. Div. ION (ION GPS 2001)*, Salt Lake City, UT, pp. 1952-1960, Sep. 2001, http://giftet.com/Progri/Progri_2001_09_03_ION_GPS.PDF. (Best Student Paper Award)

[6] I. Progri, W.R. Michalson, M.C. Bromberg, "A DSSS/CDMA/FDMA indoor geolocation system," in *Proc. ION-GPS*, Portland, OR, pp. 155-164, Sep. 2002, http://giftet.com/Progri/Progri_2002_09_01_ION_GPS.pdf.

[7] I. Progri, W.R. Michalson, G. Bogdanov, V.C. Ramanna, "An investigation of a GPS adaptive temporal selective attenuator," *Navigation*, vol. 49, no. 3, pp. 137-147, fall 2002, DOI: http://dx.doi.org/10.1002/j.2161-4296.2002.tb00263.x, http://giftet.com/Progri/Progri_2002_fall_Navigation.pdf.

[8] I. Progri, W.R. Michalson, D. Cyganski, "An OFDM/FDMA indoor geolocation system," in *Proc. ION-NTM 2003*, Anaheim, CA, pp. 272-281, Jan. 2003, http://giftet.com/Progri/Progri_2003_01_01_ION_NTM.pdf.

[9] I. Progri, "An assessment of indoor geolocation systems," *Ph.D. Dissertation*, Worcester Polytechnic Institute, 408 pg., May 2003, URL: http://giftet.com/Progri/Progri_2003_05_Ph.D._Dissertation.pdf.

[10] I. Progri, W.R. Michalson, D. Cyganski, "An OFDM/FDMA indoor geolocation system," *Navigation*, vol. 51, no. 2, pp. 133-142, summer 2004, DOI: http://dx.doi.org/10.1002/j.2161-4296.2004.tb00346.x, http://giftet.com/Progri/Progri_2004_summer_Navigation.pdf.

[11] G. Gao, "INS-assisted high sensitivity GPS receivers for degraded signal navigation," *Ph.D. Dissertation*, (Published as Reports Number 20252), Department of Geomatics Engineering, University of Calgary, Canada, Feb. 2007. (Available at http:\plan.geomatics.ucalgary.ca).

[12] I. Progri, *Geolocation of RF Signals—Principles and Simulations.* 1st ed., New York, NY: Springer Science & Business Media, LLC, 330 pg., Jan. 2011, DOI: http://doi.org/10.1007/978-1-4419-7952-0, URL: http://springer.com/engineering/electronics/book/978-1-4419-7951-3.

[13] I. Progri, *Indoor Geolocation Systems—Theory and Applications*. *I*, 1st ed., Worcester, MA: Giftet Inc., ~800 pp., ~ 2024 (not yet available in print).

# 6 Appendix A: No Noise Infinite Bandwidth

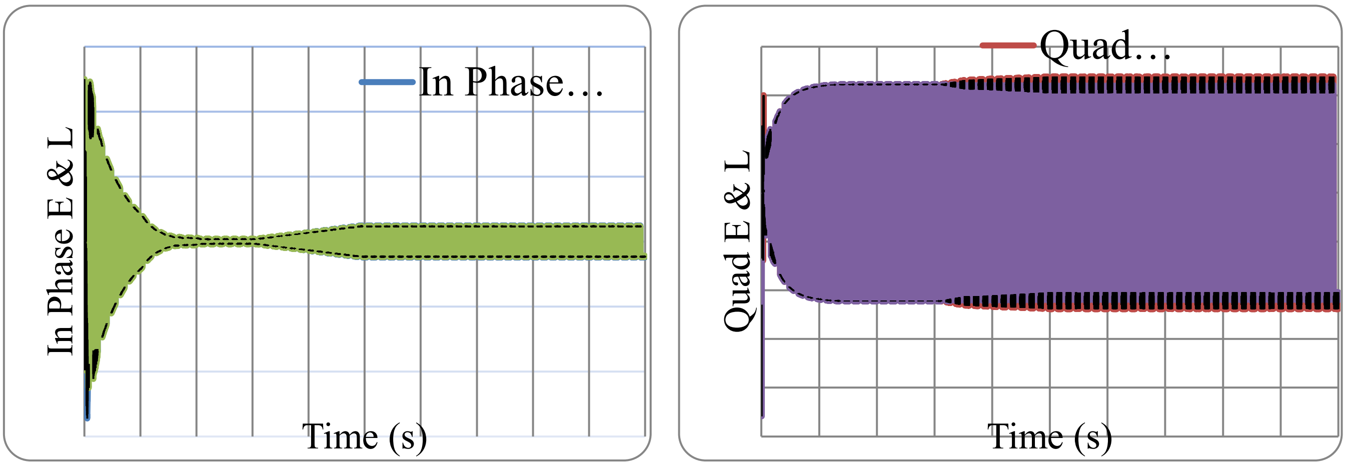


FIGURE 2: In phase (left) and quadrature (right) early and late for T = 1 ms and $B_n$ = 1 Hz (No Noise, B = 8 MHz, Stable)..

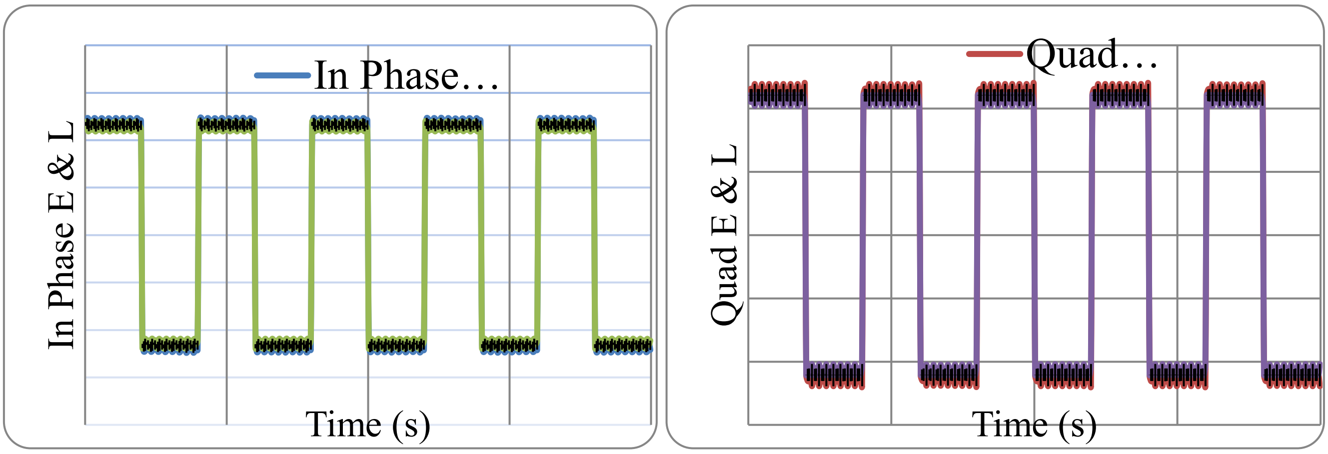


FIGURE 3: Same as Fig. 2 zoom 1.

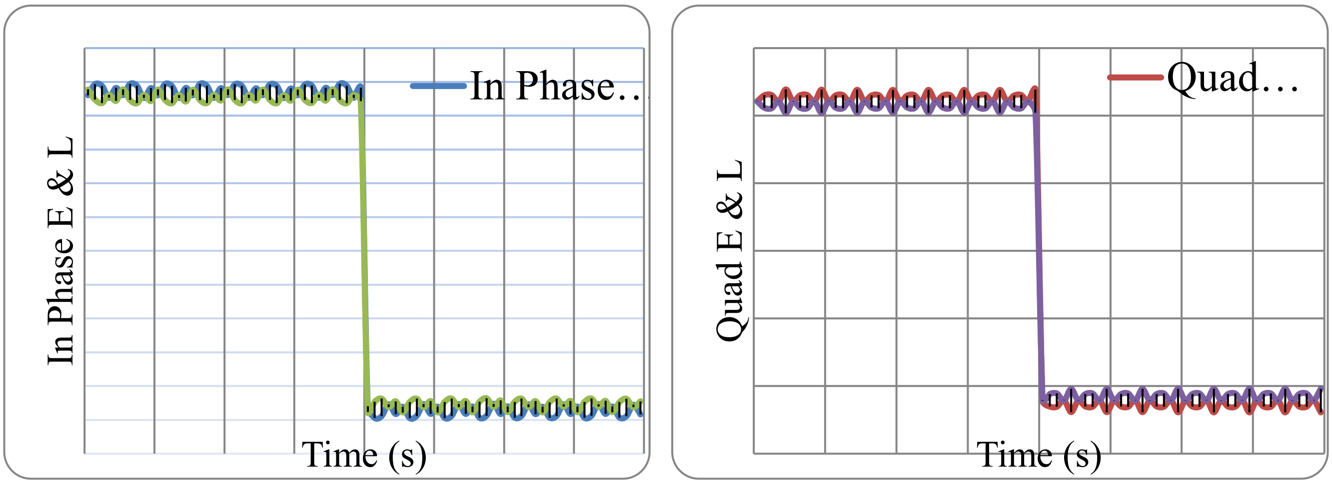


FIGURE 4: Same as Fig. 2 zoom 2.

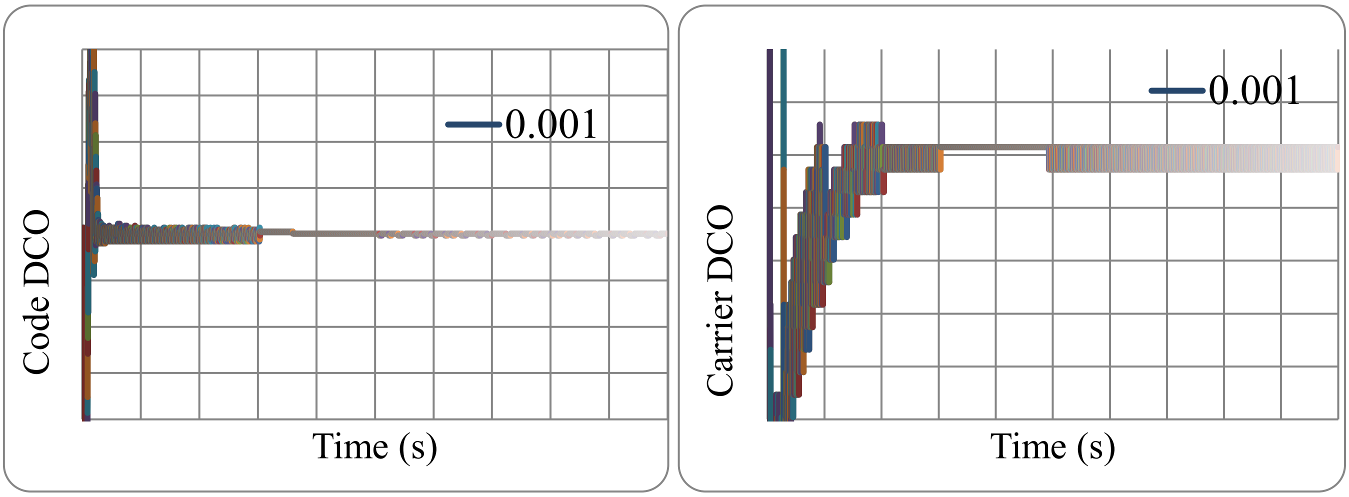


FIGURE 5: Code DCO (left) and Carrier DCO (right) for T = 1 ms and $B_n$ = 1 Hz (No Noise, B = 8 MHz, Stable).

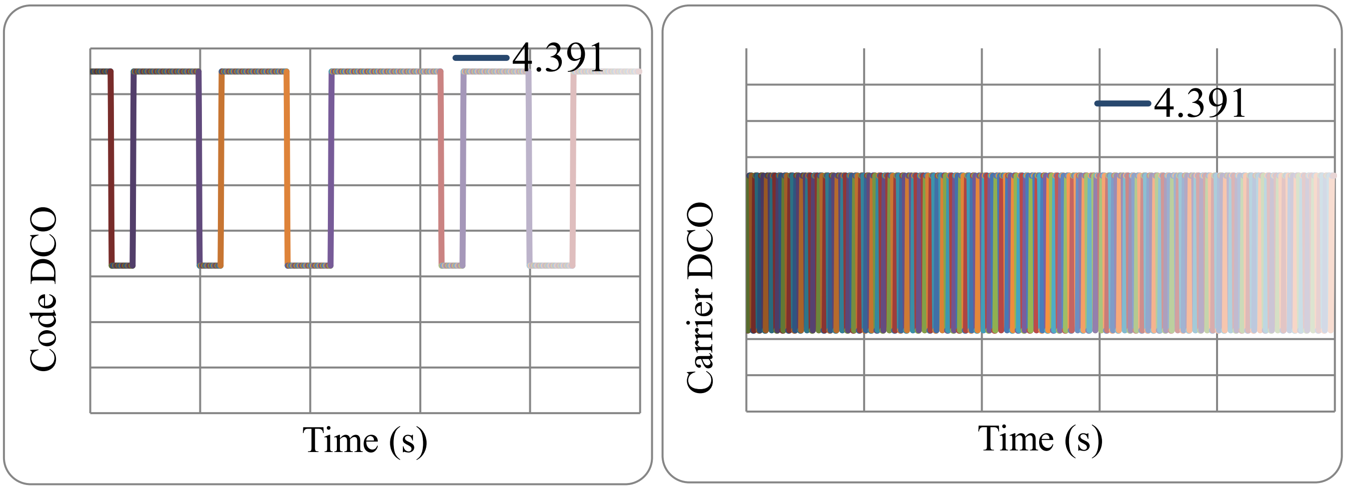


FIGURE 6: Same as Fig. 5 zoom 1.

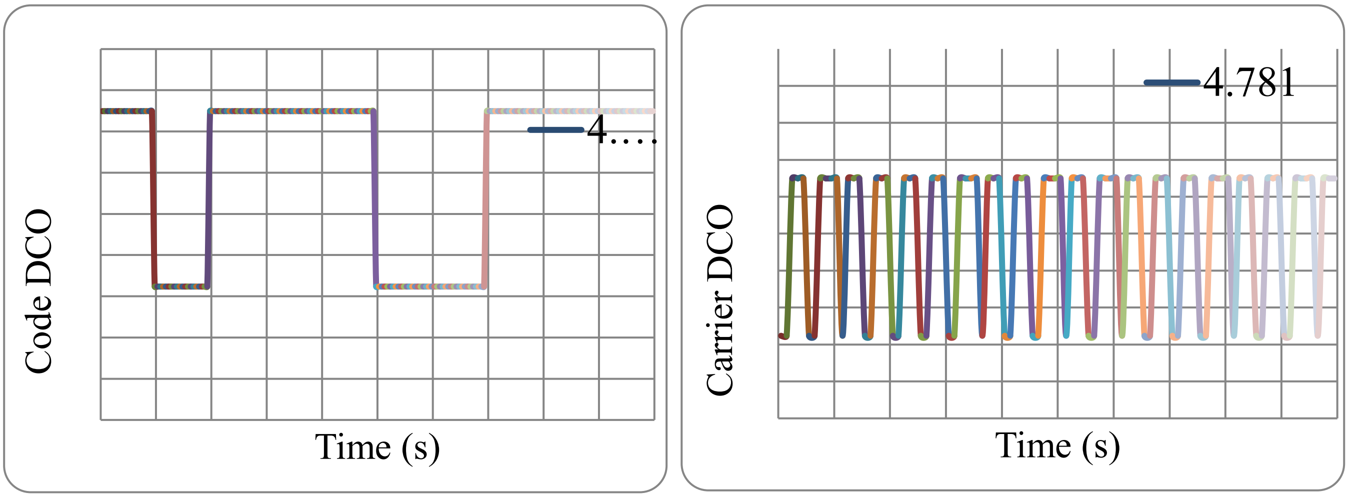


FIGURE 7: Same as Fig. 5 zoom 2.

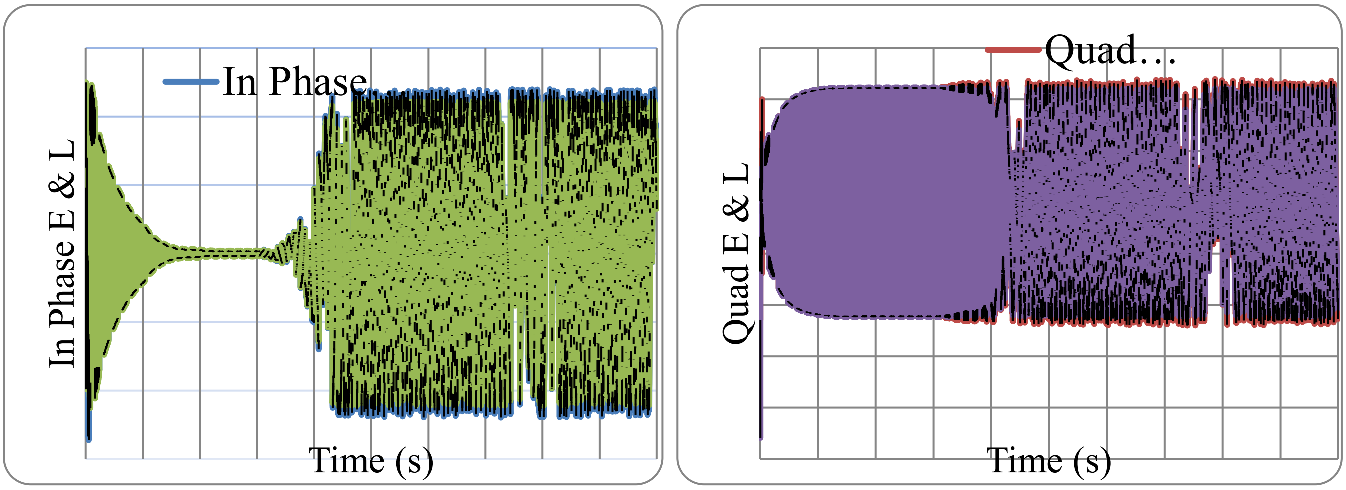


FIGURE 8: In phase (left) and quadrature (right) early and late for T = 20 ms and $B_n$ = 50 Hz (No Noise, B = 8 MHz, Unstable).

# 7 Appendix B: Real GPS signal with noise

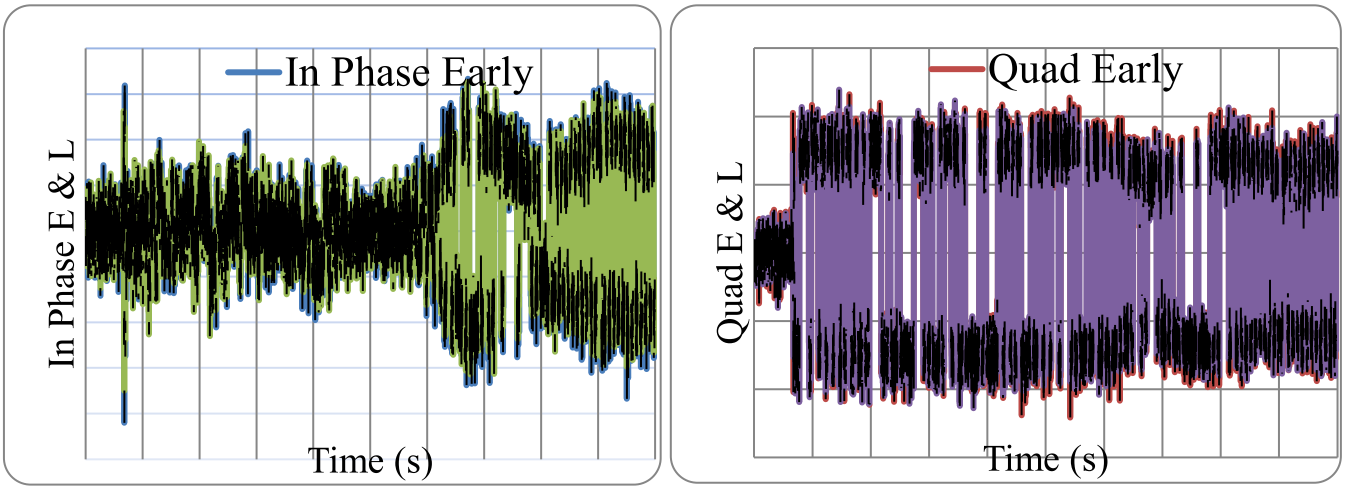


FIGURE 9: In phase (left) and quadrature (right) early and late for T = 1 ms and $B_n$ = 1 Hz (with noise, B = 16 MHz, stable)..

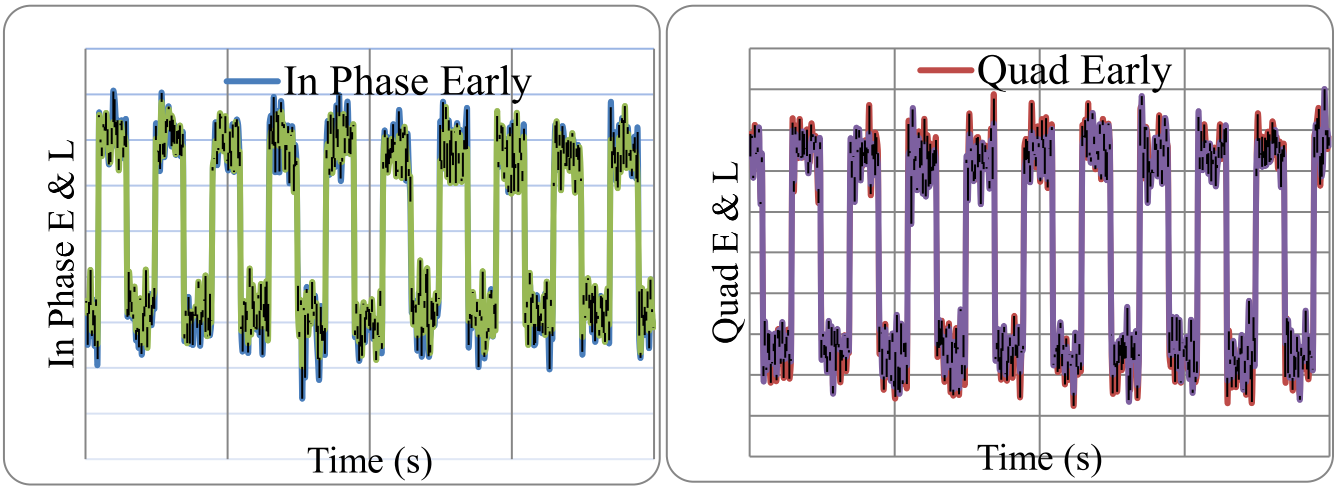


FIGURE 10: Same as Fig. 9 zoom 1

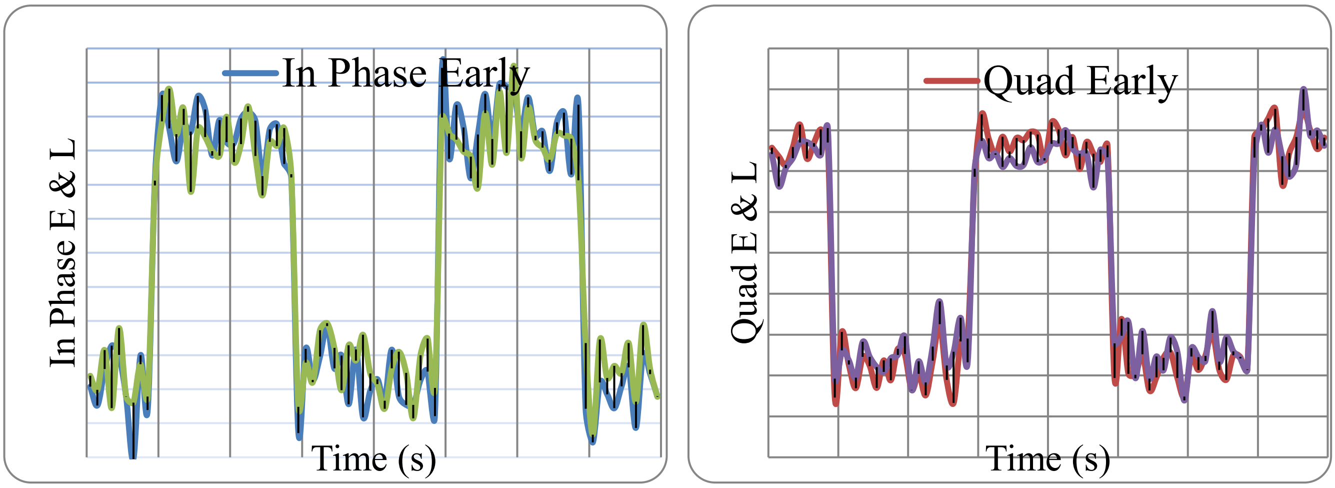


FIGURE 11: Same as Fig. 9 zoom 2.

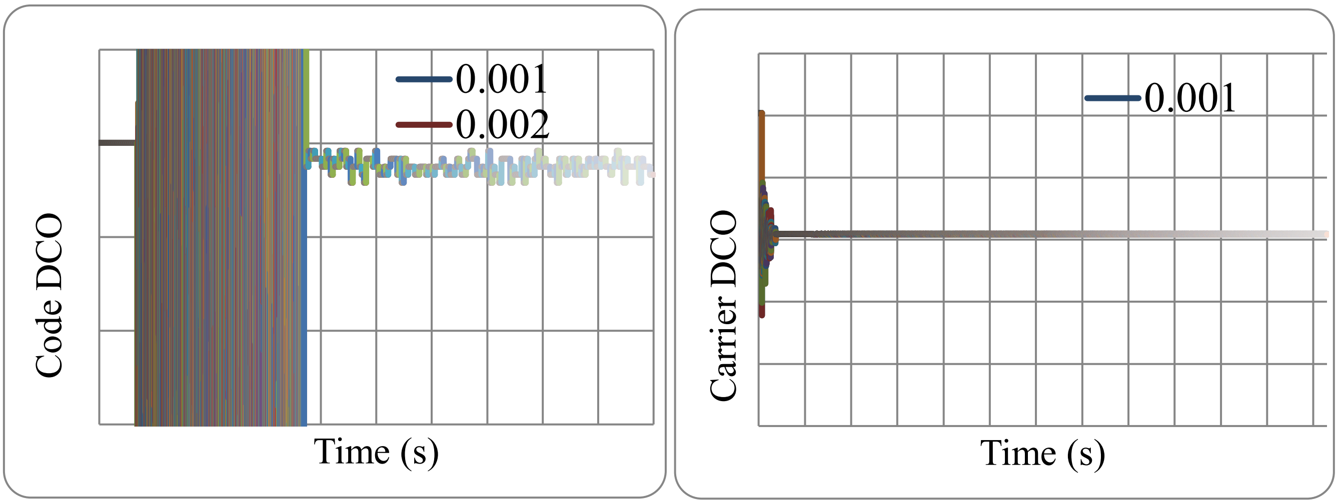


FIGURE 12: Code DCO (left) and carrier DCO (right) for T = 1 ms and $B_n$ = 1 Hz (with noise, B = 16 MHz, stable).

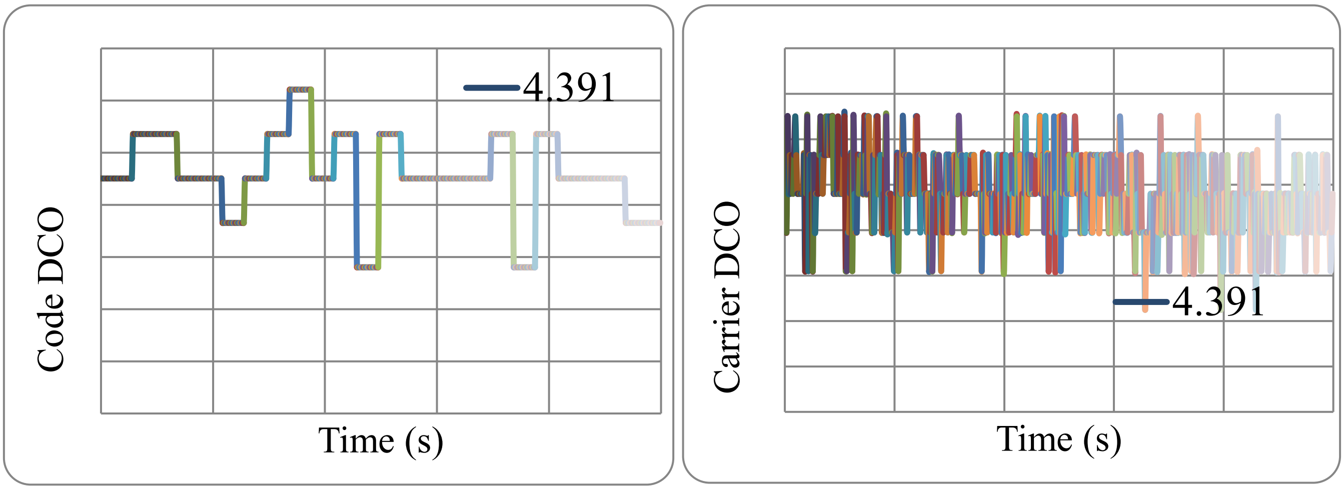


FIGURE 13: Same as Fig. 12 zoom 1.

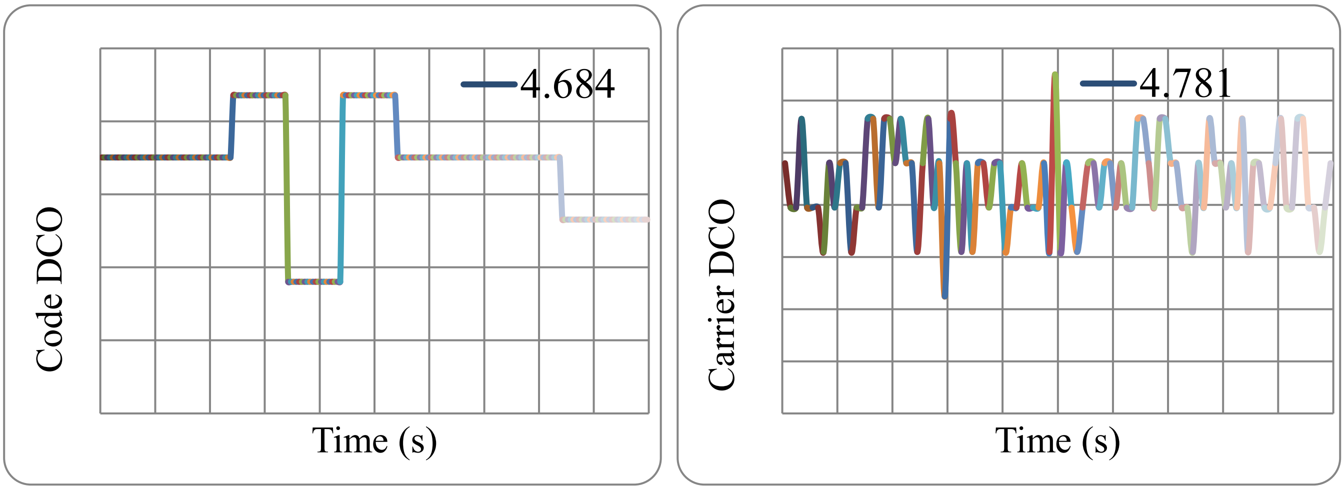


FIGURE 14: Same as Fig. 12 zoom 2.

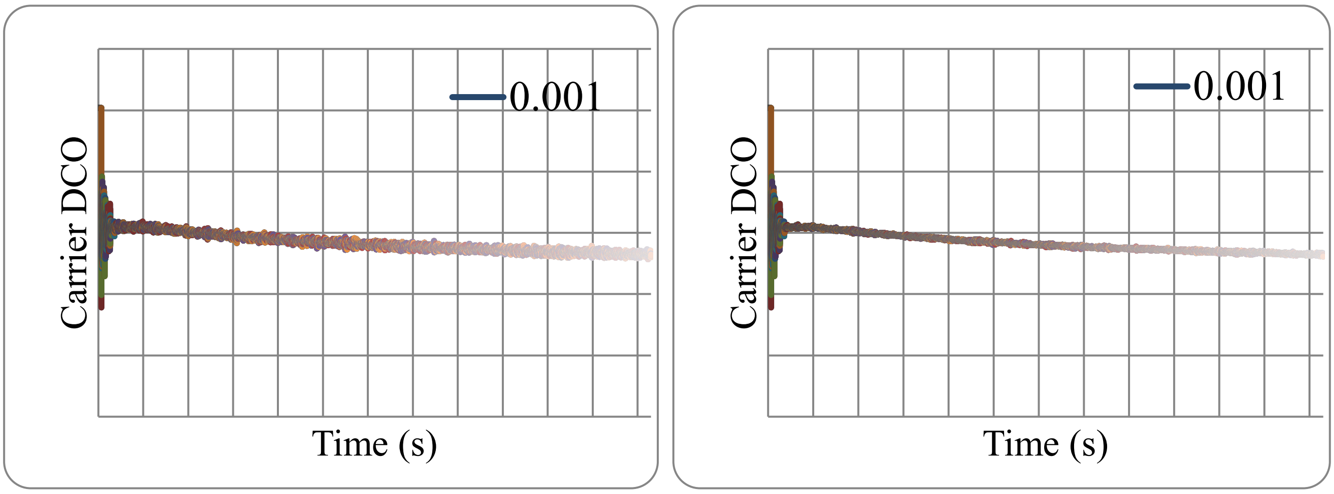


FIGURE 15: Carrier DCO for T = 10 ms, $B_n$ = 50 Hz (left) and T = 20 ms, $B_n$ = 25 Hz (right) (with noise, B = 16 MHz, marginally stable).

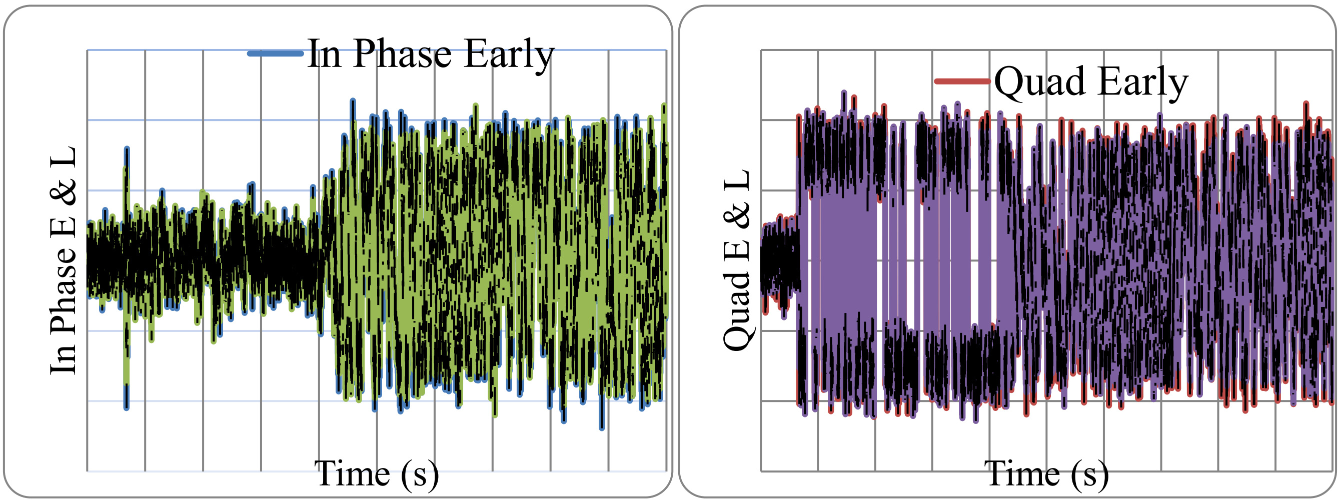


FIGURE 16: In phase (left) and quadrature (right) early and late for T = 20 ms and $B_n$ = 50 Hz (with noise, B = 16 MHz, unstable).

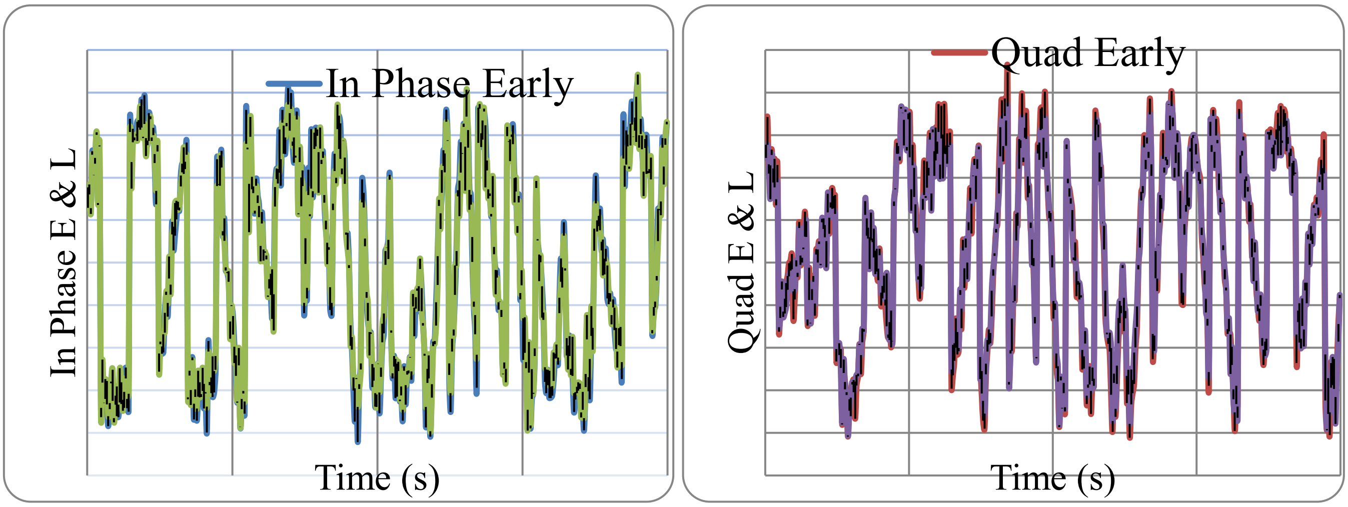


FIGURE 17: Same as Fig. 16 zoom 1.

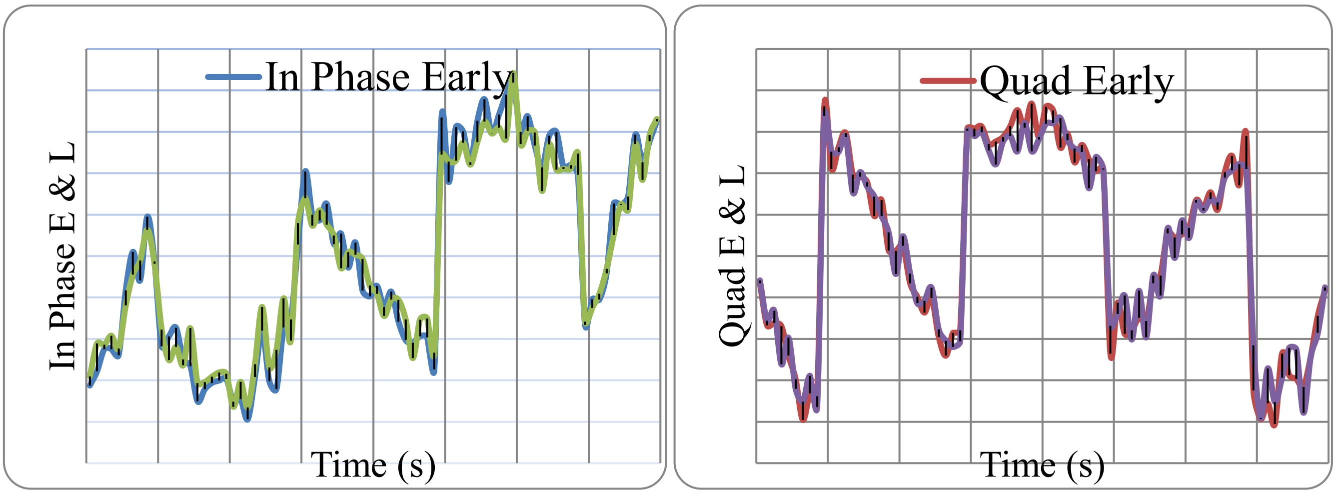


FIGURE 18: Same as Fig. 16 zoom 2.

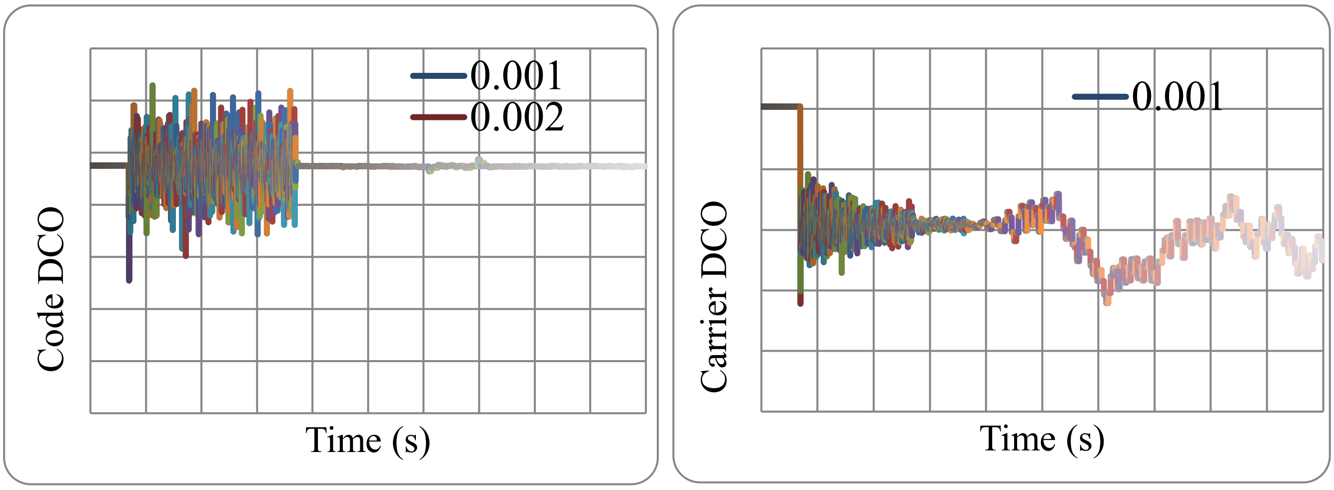


FIGURE 19: Code DCO (left) and Carrier DCO (right) for T = 20 ms and $B_n$ = 50 Hz (with noise, B = 16 MHz, unstable).

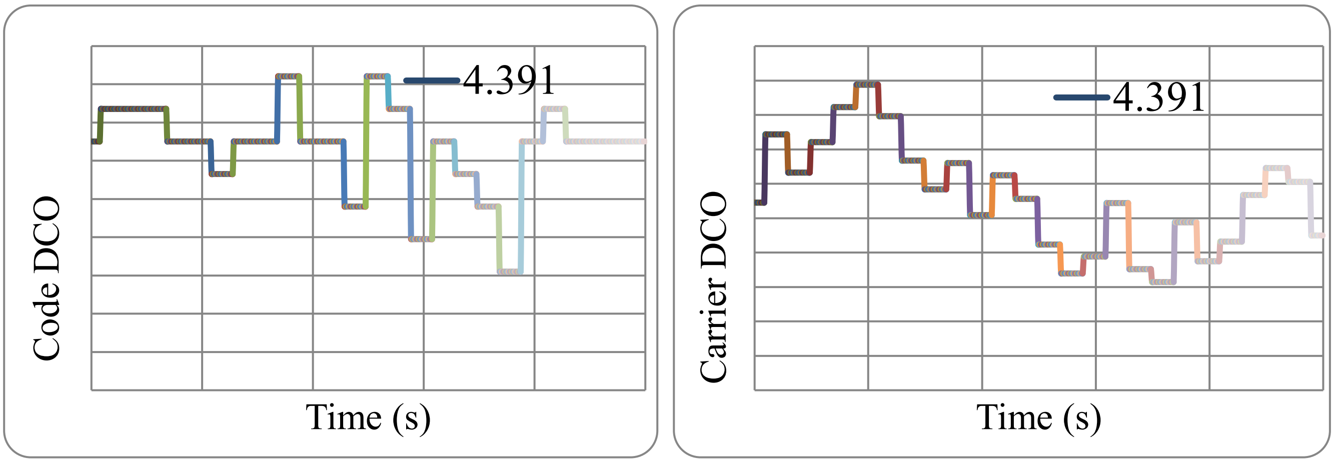


FIGURE 20: Same as Fig. 19 zoom 1.

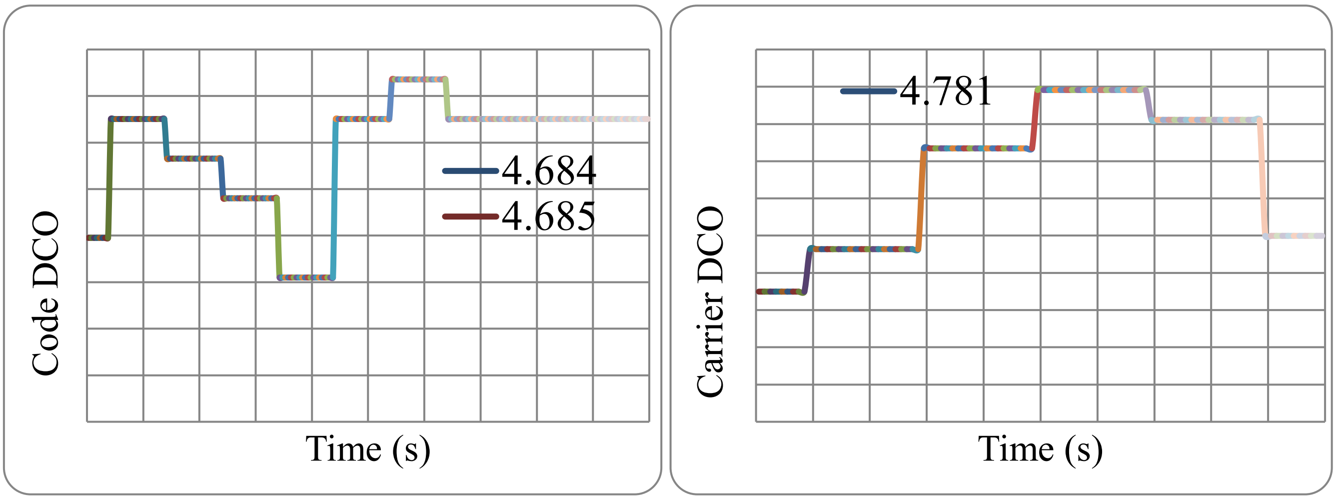


FIGURE 21: Same as Fig. 19 zoom 2.

[i] This article was originally published in Progri et al., (2007, [1]). This is a significantly improved revision of the same ION GNSS 2007 conference paper. This journal paper includes a major revision of the implementation and testing and of the interpretation of the results.